

---

# Mining gold from implicit models to improve likelihood-free inference

---

**Johann Brehmer**  
New York University

**Gilles Louppe**  
University of Liège

**Juan Pavez**  
Federico Santa María  
Technical University

**Kyle Cranmer**  
New York University

## Abstract

Simulators often provide the best description of real-world phenomena. However, they also lead to challenging inverse problems because the density they implicitly define is often intractable. We present a new suite of simulation-based inference techniques that go beyond the traditional Approximate Bayesian Computation approach, which struggles in a high-dimensional setting, and extend methods that use surrogate models based on neural networks. We show that additional information, such as the joint likelihood ratio and the joint score, can often be extracted from simulators and used to augment the training data for these surrogate models. Finally, we demonstrate that these new techniques are more sample efficient and provide higher-fidelity inference than traditional methods.

## 1 Introduction

In many areas of science, complicated real-world phenomena are best described through computer simulations. Typically, the simulators implement a stochastic generative process in the “forward” mode based on a well-motivated mechanistic model with parameters  $\theta$ . While the simulators can generate samples of observations  $x \sim p(x|\theta)$ , they typically do not admit a tractable likelihood (or density)  $p(x|\theta)$ . Probabilistic models defined only via the samples they produce are often called implicit models. Implicit models lead to intractable inverse problems, which is a barrier for statistical inference of the parameters  $\theta$  given observed data. These problems arise in fields as diverse as particle physics, epidemiology, and population genetics, which has motivated the development of *likelihood-free inference* algorithms such as Approximate Bayesian Computation (ABC) [1–4] and neural density estimation (NDE) techniques [5–25].

We present a suite of new techniques for likelihood-free inference. They are aimed at a broad class of simulator-based inference problems where additional information that characterizes the latent process can be extracted from the simulator, as we explain in Sec. 3. In Sec. 4 we show that this augmented data can be used to train neural network surrogates that estimate the likelihood  $p(x|\theta)$  or likelihood ratio  $r(x|\theta_0, \theta_1) = p(x|\theta_0)/p(x|\theta_1)$ . This provides the key quantity needed for both frequentist and Bayesian inference procedures. The resulting methods provide a significant increase in sample efficiency and quality of the resulting inference compared to previous techniques, as we demonstrate in a range of experiments in Sec. 5.

## 2 Related work

Techniques for simulator-based inference can be divided into two broad categories. The first category uses the simulator directly during inference, while the second uses the simulator to construct or train a tractable surrogate model that is used during inference. We also find strong connections between simulator-based inference and learning in implicit generative models [26], such as GANs, with a considerable amount of cross-pollination between these areas.

**Approximate Bayesian Computation (ABC).** A particularly ubiquitous method is Approximate Bayesian Computation [1, 2], a Bayesian sampling technique in which the likelihood is approximated by comparing data generated from the simulator to the observed data. This approach requires introducing a kernel  $K_\epsilon(x, x_{\text{obs}})$ , which defines a notion of distance between the simulated data  $x$  and the observed data  $x_{\text{obs}}$ . This approximate inference method is exact in the limit  $\epsilon \rightarrow 0$ . However, it scales poorly when  $x$  is high-dimensional, thus much of the research in ABC is focused on finding appropriate summary statistics. Relevant work includes classifier ABC [19], which relies on a classifier to estimate the discrepancy between the observed data and the model distribution, and Hamilto-

nian ABC [27], which makes use of finite differences through the simulator to estimate gradients with respect to  $\theta$ . Reference [28] introduces an  $\epsilon$ -free exact inference approach, but it is restricted to differentiable generative models.

**Probabilistic programming (PPS).** Probabilistic programming systems represent another class of methods that use the simulator directly during inference [29, 30]. These techniques are deeply integrated into the control flow of the program, but still require a tractable likelihood term or ABC-like kernel to compare the simulated data  $x$  and the observed data  $x_{\text{obs}}$ . While our work will not utilize probabilistic programming, there is commonality in the notion of a non-standard interpretation of the simulator code to produce a non-standard output.

**The likelihood ratio trick (LRT).** A surrogate model for the likelihood ratio  $\hat{r}(x|\theta_0, \theta_1)$  can be defined by training a probabilistic classifier to discriminate between two equal-sized samples  $\{x_i\} \sim p(x|\theta_0)$  and  $\{x_i\} \sim p(x|\theta_1)$ . The binary cross-entropy loss

$$L_{\text{XE}} = -\mathbb{E}_{p(x|\theta)\pi(\theta)}[\mathbb{1}(\theta = \theta_1) \log \hat{s}(x|\theta_0, \theta_1) + \mathbb{1}(\theta = \theta_0) \log(1 - \hat{s}(x|\theta_0, \theta_1))] \quad (1)$$

is minimized by the optimal decision function

$$s(x|\theta_0, \theta_1) = \frac{p(x|\theta_1)}{p(x|\theta_0) + p(x|\theta_1)}. \quad (2)$$

Since  $r(x|\theta_0, \theta_1) \equiv p(x|\theta_0)/p(x|\theta_1) = (1 - s)/s$ , the likelihood ratio can be estimated from the classifier decision function as

$$\hat{r}(x|\theta_0, \theta_1) = \frac{1 - \hat{s}(x|\theta_0, \theta_1)}{\hat{s}(x|\theta_0, \theta_1)}. \quad (3)$$

This ‘‘likelihood ratio trick’’ or ‘‘density ratio trick’’ is widely appreciated [9, 20, 26, 31].

An improvement to this basic idea was introduced in Refs. [9, 32]. In practice, not all probabilistic classifiers trained to separate samples from  $\theta_0$  and  $\theta_1$  learn the decision function given in Eq. (2). As long as the classifier decision function is a monotonic function of the likelihood ratio, this relation can be restored through a calibration procedure, which substantially increases the applicability of the likelihood ratio trick. We use the term CARL (Calibrated approximate ratios of likelihoods) to describe likelihood ratio estimators based on classifiers with a subsequent calibration.

**Neural density estimation (NDE).** More recently, several methods for conditional density estimation have been proposed, often based on neural networks [5–8, 11–18, 20–25]. These provide flexible models for  $\hat{p}(x|\theta)$ , and training them by minimizing the

negative log likelihood

$$L_{\text{MLE}} = -\mathbb{E}_{p(x|\theta)}[\log \hat{p}(x|\theta)] \quad (4)$$

with a sufficiently flexible density estimator will approximate  $p^*(x|\theta) = p(x|\theta)$ .

One particularly interesting class of neural density estimation techniques are normalizing flows [6, 8, 11, 22–25]. In this approach, the distribution of a target variable is modeled as a sequence of invertible transformations applied to a simple base density. The target density is then given by the Jacobian determinant of the transformation. Closely related, autoregressive models [7, 15–18] factorize a target density as a sequence of simpler conditional densities.

**Novel contributions.** The most important novel contribution that differentiates our work from the existing methods is the observation that additional information can be extracted from the simulator, and that this ‘‘augmented’’ data can dramatically improve sample efficiency and quality of likelihood-free inference. We playfully introduce the analogy of mining gold as this augmented data requires work to extract and is very valuable.

Concurrently, the application of these methods to a specific class of problems in particle physics has been discussed in Refs. [33, 34]. The present manuscript is meant to serve as the primary reference for these new techniques. It is addressed to the broader community and requires weaker assumptions than those made in the physics context. We also introduce an entirely new algorithm called SCANDAL, for which we provide the first experimental results.

### 3 Extracting more information from the simulator

Typically the setting of likelihood-free inference methods assumes that the only available output from the simulator are samples of observations  $x \sim p(x|\theta)$ . However, we will show that in many cases additional information can be extracted from the simulator, even though the implicit density is intractable. Let the generative process be characterized by some set of latent variables  $z$  such that

$$p(x|\theta) = \int dz p(x, z|\theta). \quad (5)$$

Often the likelihood is intractable exactly because the latent space  $z$  is enormous and it is unfeasible to explicitly calculate this integral. In real-world scientific simulators, the trajectory for a single observation can involve many millions of latent variables.

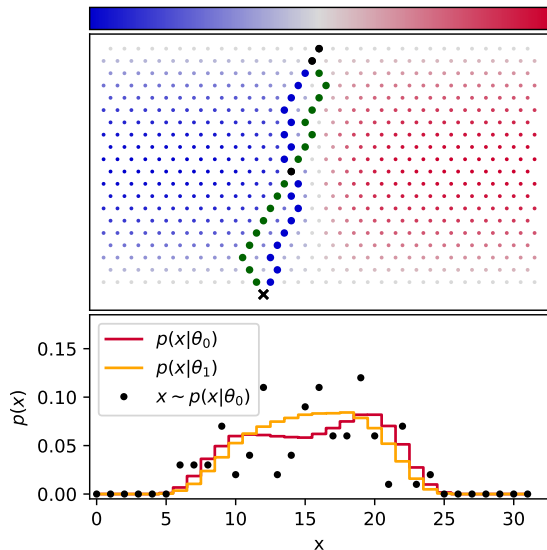


Figure 1: A toy simulation generalizing the Galton board where the transitions are biased left (blue) or right (red) depending on the nail position and the value of  $\theta$ . Two example latent trajectories  $z$  are shown (blue and green), leading to the same observed value of  $x$ . Below, the distribution for  $\theta_0 = -0.8$  and  $\theta_1 = -0.6$  (orange and red histograms). Finally, an example empirical distribution from 100 runs of the simulator with  $\theta_0$  shows that the sample variance is much larger than the differences from  $\theta_0$  vs.  $\theta_1$ .

As a motivating example, consider the simulation for a generalization of the Galton board, in which a set of balls is dropped through a lattice of nails ending in one of several bins denoted by  $x$ . The Galton board is commonly used to demonstrate the central limit theorem, and if the nails are uniformly placed such that the probability of bouncing to the left is  $p$ , the sum over the latent space is tractable analytically and the resulting distribution of  $x$  is a binomial distribution with  $N_{\text{rows}}$  trials and probability  $p$  of success. However, if the nails are not uniformly placed, and the probability of bouncing to the left is an arbitrary function of the nail position and some parameter  $\theta$ , the resulting distribution requires an explicit sum over the latent paths  $z$  that might lead to a particular  $x$ . Such a distribution would become intractable as  $N_{\text{rows}}$ , the size of the lattice of nails, increases. Figure 1 shows an example of two latent trajectories that lead to the same  $x$ . In this toy example, the probability  $p(z_h, z_v, \theta)$  of going left is given by  $(1 - f(z_v))/2 + f(z_v)\sigma(5\theta(z_h - 1/2))$ , where  $f(z_v) = \sin(\pi z_v)$ ,  $\sigma$  is the sigmoid function, and  $z_h$  and  $z_v$  are the horizontal and vertical nail positions normalized to  $[0, 1]$ . This leads to a non-trivial  $p(x|\theta)$ , which can even be bimodal. Code for simulation and inference in this problem is available at Ref. [35].

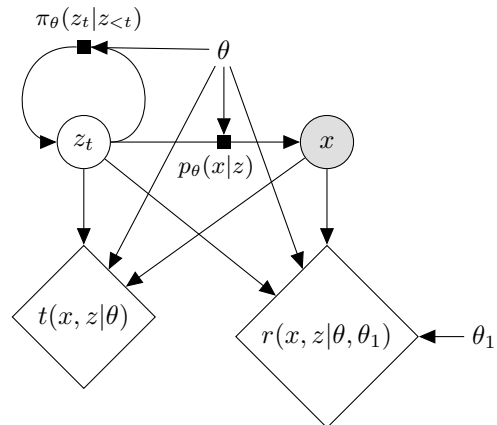


Figure 2: A graphical model representation of a density defined implicitly by a stochastic simulator where the latent state  $z_t$  evolves sequentially according to a policy  $p_\theta(z_t|z_{<t}, \theta)$  and final observation model  $p_\theta(x|z, \theta)$ . The joint score  $t(x, z|\theta)$  and joint ratio  $r(x, z|\theta, \theta_1)$  are tractable deterministic functions that can be extracted from the simulator code.

Figure 1 shows that a large number of samples from the simulator are needed to reveal the differences in the distribution of  $x$  for small changes in  $\theta$  – the number of samples needed grows like  $(p/\Delta p)^2$ . Moreover, this toy simulation is representative of many real-world simulators in that it is composed of non-differentiable control-flow elements. This poses a difficulty, making methods based on  $\nabla_{z_x}$  [28] and  $\nabla_{\theta} x$  inapplicable, which previously motivated techniques such as Adversarial Variational Optimization [21].

The key observation that is the starting point of our new inference methods is the following: While  $p(x|\theta)$  is intractable, the *joint score*

$$t(x, z|\theta_0) \equiv \nabla_{\theta} \log p(x, z|\theta) \Big|_{\theta_0}. \quad (6)$$

can be computed by accumulating the factors  $\nabla_{\theta} \log p(z_h, z_v|\theta)$  as the simulation runs forward through its control flow conditioned on the random trajectory  $z$ . A similar trick can be applied to extract the *joint likelihood ratio*

$$r(x, z|\theta_0, \theta_1) \equiv \frac{p(x, z|\theta_0)}{p(x, z|\theta_1)}. \quad (7)$$

In analogy to the Galton board toy example, even complicated real-world simulators often allow us to accumulate these factors as they run, and to calculate the joint score and joint likelihood ratio conditional on a particular stochastic execution trace  $z$ . We will demonstrate this with two more examples in Sec. 5.

Figure 2 presents a graphical model that abstracts the simulation to be a probabilistic sequence of latent

states  $z_t$ . The latent space structure can involve discrete and continuous components and is derived from the control flow of the simulation code. The mechanistic model implemented by the simulator describes a particular probabilistic transition  $\pi_\theta(z_t|z_{<t})$ , which can be viewed as a parameterized policy for taking the action  $z_t$  given the past  $z_{<t}$ . Finally, the simulation emits a sampled observation based on  $p_\theta(x|z)$ . While  $p(x|\theta)$  is intractable due to the integration over the latent space, it is possible to calculate how much more or less likely a particular trajectory through the simulator would be if one changed  $\theta$ . Moreover, this relative change can efficiently be accumulated as the simulation transitions from  $z_t \rightarrow z_{t+1}$ . This is essentially the same observation as the policy gradient used in REINFORCE [36]; however, instead of trying to optimize  $\theta$  via a stochastic gradient estimate of some reward function, we will simply augment the data generated by the simulator with the joint score. Similarly, there is a large class of problems in which one can extract the joint likelihood ratio from the simulator even though  $p(x|\theta)$  is intractable.

## 4 Learning from augmented data

### 4.1 Key idea

From now on we assume the setting outlined above, in which the simulator provides not only observations  $x_i$ , but also the joint likelihood ratio  $r(x_i, z_i|\theta_0, \theta_1)$  and the joint score  $t(x_i, z_i|\theta_0)$ , both conditional on the unobservable latent variables  $z_i$ . How can this “augmented data” be used to estimate the likelihood ratio function  $r(x|\theta_0, \theta_1)$ ? The relation between  $r(x, z|\theta_0, \theta_1)$  and  $r(x|\theta_0, \theta_1)$  is not trivial — the integral of the ratio is not the ratio of the integrals! Similarly, how can the joint score be used to estimate the intractable score function

$$t(x|\theta_0) \equiv \nabla_\theta \log p(x|\theta) \Big|_{\theta_0} ? \quad (8)$$

The integral of the log is not the log of the integral!

Consider the squared error of a function  $\hat{g}(x)$  that only depends on the observable  $x$ , but is trying to approximate a function  $g(x, z)$  that also depends on the latent variable  $z$ ,

$$L_{\text{MSE}} = \mathbb{E}_{p(x, z|\theta)} \left[ (g(x, z) - \hat{g}(x))^2 \right]. \quad (9)$$

The minimum-mean-squared-error prediction of  $g$  is given by the conditional expectation

$$g^*(x) = \mathbb{E}_{p(z|x, \theta)} [g(x, z)]. \quad (10)$$

Identifying  $g(x, z)$  with the joint likelihood ratio

$r(x, z|\theta_0, \theta_1)$  and  $\theta = \theta_1$ , we define

$$L_r = \mathbb{E}_{p(x, z|\theta_1)} \left[ (r(x, z|\theta_0, \theta_1) - \hat{r}(x))^2 \right], \quad (11)$$

which is minimized by

$$r^*(x) = \mathbb{E}_{p(z|x, \theta_1)} [r(x, z|\theta_0, \theta_1)] = r(x|\theta_0, \theta_1). \quad (12)$$

Similarly, by identifying  $g(x, z)$  with the joint score  $t(x, z|\theta_0)$  and setting  $\theta = \theta_0$ , we define

$$L_t = \mathbb{E}_{p(x, z|\theta_0)} \left[ (t(x, z|\theta_0) - \hat{t}(x|\theta_0))^2 \right], \quad (13)$$

which is minimized by

$$t^*(x) = \mathbb{E}_{p(z|x, \theta_0)} [t(x, z|\theta_0)] = t(x|\theta_0). \quad (14)$$

These loss functionals are useful because they allow us to transform  $t(x, z|\theta_0)$  into  $t(x|\theta_0)$  and  $r(x, z|\theta_0, \theta_1)$  into  $r(x|\theta_0, \theta_1)$ : we are able to regress on these two intractable quantities! This is what makes the joint score and joint likelihood ratio the gold worth mining.

### 4.2 Learning the likelihood ratio

Based on this observation we introduce a family of new likelihood-free inference techniques. They fall into two categories. We first discuss a class of algorithms that uses the augmented data to learn a surrogate model for any likelihood  $p(x|\theta)$  or likelihood ratio  $r(x|\theta_0, \theta_1)$ . In Section 4.3 we will define a second class of methods that is based on a local expansion of the model around some reference parameter point.

The simulators we consider in this work do not only implicitly define a single density  $p(x)$ , but a family of densities  $p(x|\theta)$ . The parameters  $\theta$  may potentially belong to a high-dimensional parameter space. For inference models based on surrogate models, there are two broad strategies to model this dependence. The first is to estimate  $p(x|\theta)$  or the likelihood ratio  $r(x|\theta_0, \theta_1)$  for specific values of  $\theta$  or pairs  $(\theta_0, \theta_1)$ . This may be done via a pre-defined set of  $\theta$  values or on-demand using an active-learning iteration.

We follow a second approach, in which we train *parameterized estimators* for the full model  $\hat{p}(x|\theta)$  or  $\hat{r}(x|\theta_0, \theta_1)$  as a function of both the observables  $x$  and the parameters  $\theta$  [9, 37]. The training data then consists of a number of samples, each generated with different values of  $\theta_0$  and  $\theta_1$ , and the parameter values are used as additional inputs to the surrogate model. When modeling the likelihood ratio, the reference hypothesis  $\theta_1$  in the denominator of the likelihood ratio can be kept at a fixed reference value (or a marginal model with some prior  $\pi(\theta_1)$ ), and only the  $\theta_0$  dependence is modeled by the network. This approach encourages the

estimator to learn the typically smooth dependence of the likelihood ratio on the parameters of interest from the training data and borrow power from neighboring training data.

**ROLR (Regression On Likelihood Ratio):** In this most straightforward inference algorithm based on the augmented data, we first draw a number of parameter points  $(\theta_0, \theta_1)$  with  $\theta_i \sim \pi_i(\theta_i)$ . For each pair  $(\theta_0, \theta_1)$ , we run the simulator both for  $\theta_0$  and for  $\theta_1$ , labelling the samples with  $y = 0$  and  $y = 1$ , respectively. In addition to samples  $x \sim p(x|\theta_y)$  we also extract the joint likelihood ratio  $r(x, z|\theta_0, \theta_1)$ .

An expressive regressor  $\hat{r}(x|\theta_0, \theta_1)$  (e.g. a neural network) is trained by minimizing the squared error loss

$$L_{\text{ROLR}}[\hat{r}] = \frac{1}{N} \sum_i \left( y_i |r(x_i, z_i) - \hat{r}(x_i)|^2 + (1 - y_i) \left| \frac{1}{r(x_i, z_i)} - \frac{1}{\hat{r}(x_i)} \right|^2 \right). \quad (15)$$

Here and in the following the  $\theta$  dependence is implicit to reduce the notational clutter.

Both terms in this loss function are estimators of Eq. (11) (in the second term we switch  $\theta_0 \leftrightarrow \theta_1$  to reduce the variance by mapping out other regions of  $x$  space). As we showed in the previous section, this loss function is, at least in the limit of infinite data, minimized by the likelihood ratio  $r(x|\theta_0, \theta_1)$ . A regressor trained in this way thus provides an estimator for the likelihood ratio and can be used for frequentist or Bayesian inference methods.

**RASCAL (Ratio And Score Approximate Likelihood ratio):** If such a likelihood ratio regressor is differentiable (as is the case for neural networks) with respect to  $\theta$ , we can calculate the predicted score  $\hat{t}(x|\theta_0) = \nabla_{\theta_0} \log \hat{r}(x|\theta_0, \theta_1)$ . For a perfect likelihood ratio estimator,  $\hat{t}(x|\theta_0)$  minimizes the squared error with respect to the joint score, see Eq. (14). Turning this argument around, we can improve the training of a likelihood ratio estimator by minimizing the combined ratio and score loss

$$L_{\text{RASCAL}}[\hat{r}] = L_{\text{ROLR}}[\hat{r}] + \alpha \frac{1}{N} \sum_i (1 - y_i) |t(x_i, z_i) - \nabla_{\theta_0} \log \hat{r}(x_i)|^2 \quad (16)$$

with a hyper-parameter  $\alpha$ .

**CASCAL (CARL And Score Approximate Likelihood ratio):** The same trick can be used to improve the likelihood ratio trick and the CARL inference

method [9, 32]. Following Eq. (3), a calibrated classifier trained to discriminate samples  $\{x_i\} \sim p(x|\theta_0)$  and  $\{x_i\} \sim p(x|\theta_1)$  provides a likelihood ratio estimator. For a differentiable parameterized classifier, we can calculate the surrogate score  $\hat{t}(x|\theta_0) = \nabla_{\theta_0} \log[(1 - \hat{s}(x|\theta_0, \theta_1))/\hat{s}(x|\theta_0, \theta_1)]$ . This allows us to train an improved classifier (and thus likelihood ratio estimator) by minimizing the combined loss

$$L_{\text{CASCAL}}[\hat{s}] = L_{\text{XE}}[\hat{s}] + \alpha \frac{1}{N} \sum_i (1 - y_i) \left| t(x_i, z_i) - \nabla_{\theta_0} \log \left[ \frac{1 - \hat{s}(x)}{\hat{s}(x)} \right] \right|^2. \quad (17)$$

**SCANDAL (Score-Augmented Neural Density Approximates Likelihood):** Finally, we can use the same strategy to improve conditional neural density estimators such as density networks or normalizing flows. If a parameterized neural density estimator  $\hat{p}(x|\theta)$  is differentiable with respect to  $\theta$ , we can calculate the surrogate score  $\hat{t}(x) = \nabla_{\theta} \log \hat{p}(x|\theta)$  and train an improved density estimator by minimizing

$$L_{\text{SCANDAL}}[\hat{p}] = L_{\text{MLE}} + \alpha \frac{1}{N} \sum_i |t(x_i, z_i) - \nabla_{\theta} \log \hat{p}(x)|^2. \quad (18)$$

Unlike the methods discussed before, this provides an estimator of the likelihood itself rather than its ratio. Depending on the architecture, the surrogate also provides a generative model.

These ideas give rise to many more possible combinations. It is for instance straightforward to combine any neural density estimator with both ratio and score information. We leave these possible extensions to future work.

### 4.3 Locally sufficient statistics for implicit models

A second class of new likelihood-free inference methods is based on an expansion of the implicit model around a reference point  $\theta_{\text{ref}}$ . Up to linear order in  $\theta - \theta_{\text{ref}}$ , we find

$$p_{\text{local}}(x|\theta) = \frac{1}{Z(\theta)} p(t(x|\theta_{\text{ref}}) | \theta_{\text{ref}}) \exp[t(x|\theta_{\text{ref}}) \cdot (\theta - \theta_{\text{ref}})] \quad (19)$$

with some normalization factor  $Z(\theta)$ . This local approximation is in the exponential family and the score vector  $t(x|\theta_{\text{ref}})$ , defined in Eq. (8), are its sufficient statistics.

For inference in a sufficiently small neighborhood around a reference point  $\theta_{\text{ref}}$ , a precise estimator of the score  $\hat{t}(x|\theta_{\text{ref}})$  therefore defines a vector of ideal

summary statistics that contain all the information in an observation  $x$  on the parameters  $\theta$ . Amazingly, the joint score together with Eqs. (13) and (14) allow us to extract sufficient statistics from an intractable, non-differentiable simulator, at least in the neighborhood of  $\theta_{\text{ref}}$ . Moreover, this local model can be estimated by running the simulator at a single value  $\theta_{\text{ref}}$ —it does not require scanning the  $\theta$  space, and thus avoids the curse of dimensionality. Based on this observation, we introduce two further inference strategies:

**SALLY (Score Approximates Likelihood Locally):** By minimizing the squared error with respect to the joint score, see Eq. (13), we train a score estimator  $\hat{t}(x|\theta_{\text{ref}})$ . In a next step, we estimate the density  $\hat{p}(\hat{t}(x|\theta_{\text{ref}})|\theta)$  through standard density estimation techniques, defining the likelihood ratio estimator  $\hat{r}(x|\theta_0, \theta_1) = \hat{p}(\hat{t}(x|\theta_{\text{ref}})|\theta_0)/\hat{p}(\hat{t}(x|\theta_{\text{ref}})|\theta_1)$ . This calibration procedure implicitly includes the effect of the normalizing constant  $Z(\theta)$ .

**SALLINO (Score Approximates Likelihood Locally IN One dimension):** The SALLY inference method requires density estimation in the estimated score space, with typically  $\dim \hat{t} \equiv \dim \theta \ll \dim x$ . But in cases with large number of parameters, it is beneficial to reduce the dimensionality even further. In the local model of Eq. (19), the likelihood ratio  $r(x|\theta_0, \theta_1)$  only depends on the scalar product between the score and  $(\theta_0 - \theta_1)$  up to an  $x$ -independent constant related to  $Z(\theta)$ . Thus, given a score estimator  $\hat{t}(x|\theta_{\text{ref}})$ , we can define the scalar function  $\hat{h}(x|\theta_0, \theta_1) \equiv \hat{t}(x|\theta_{\text{ref}}) \cdot (\theta_0 - \theta_1)$ . In the local approximation and assuming a precise estimator  $\hat{t}(x|\theta_{\text{ref}})$ , this scalar is a sufficient statistic for the 1-dimensional parameter space connecting  $\theta_0$  and  $\theta_1$ . This motivates another inference technique: again, a neural network is trained on the joint score data from the simulator to estimate the score  $\hat{t}(x|\theta_{\text{ref}})$ . The likelihood ratio is then estimated through univariate density estimation on  $\hat{h}$  as  $\hat{r}(x|\theta_0, \theta_1) = \hat{p}(\hat{h}(x|\theta_0, \theta_1)|\theta_0)/\hat{p}(\hat{h}(x|\theta_0, \theta_1)|\theta_1)$ .

The SALLY and SALLINO techniques are designed to work very well close to the reference point. The local model approximation may deteriorate further away, leading to a reduced sensitivity and weaker bounds. These approaches are simple and robust, and in particular the SALLINO algorithm scales exceptionally well to high-dimensional parameter spaces.

Table 1 summarizes six new approaches to simulator-based inference that leverage the augmented data and loss functions described above.

For all these inference strategies, the augmented data is particularly powerful for enhancing the power of simulation-based inference for small changes in the

Method	$L_{\text{XE}}$	$L_{\text{MLE}}$	$L_r$	$L_t$	$\theta$ sampling
ABC					$\theta \sim \pi(\theta)$
NDE		✓			$\theta \sim \pi(\theta)$
LRT/CARL	✓				$\theta \sim \pi(\theta)$
ROLR			✓		$\theta \sim \pi(\theta)$
RASCAL			✓	✓	$\theta \sim \pi(\theta)$
CASCAL	✓			✓	$\theta \sim \pi(\theta)$
SCANDAL		✓		✓	$\theta \sim \pi(\theta)$
SALLY				✓	$\theta = \theta_0$
SALLINO				✓	$\theta = \theta_0$

Table 1: A summary of simulator-based inference strategies including the traditional ABC method and approaches that use neural networks to learn a surrogate for amortized likelihood-free inference. Approaches based on neural density estimation and CARL only make use of the samples  $x \sim p(x|\theta)$ , while the six new methods leverage the augmented data and the loss functions  $L_r$  and  $L_t$ .

parameter  $\theta$ . When restricted to samples  $x \sim p(x|\theta)$  the variance from the simulator is a challenge. The fluctuations in the empirical density scale with the square root of the number of samples, thus large numbers of samples are required before small changes in the implicit density can faithfully be distinguished. In contrast, each sample of the joint ratio and joint score provides an exact piece of information even for arbitrarily small changes in  $\theta$ .

On the other hand, the augmented data is less powerful for deciding between model parameter points that are far apart. In this situation the joint probability distributions  $p(x, z|\theta)$  often do not overlap significantly, and the joint likelihood ratio can have a large variance around the intractable likelihood ratio  $r(x|\theta_0, \theta_1)$ . In addition, over large distances in parameter space the local model is not valid and the score does not characterize the likelihood ratios anymore, limiting the usefulness of the joint score.

## 5 Experiments

### 5.1 Generalized Galton board

We return to the motivating example in Sec. 3 and Fig. 1 and try to estimate likelihood ratios for the generalized Galton board. We use the likelihood ratio trick and a neural density estimator as baselines and compare them to the new ROLR, RASCAL, CASCAL, and SCANDAL methods. As the simulator defines a distribution over a discrete  $x$ , for the NDE and SCANDAL methods we use a neural network with a softmax

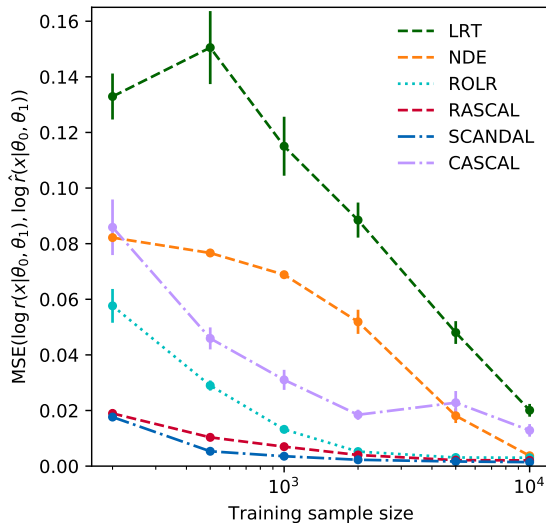


Figure 3: Galton board example. MSE on  $\log r$  vs. training sample size. We show the mean and its error based on 15 runs.

output layer over the bins to model  $\hat{p}(x|\theta)$ . All networks are explicitly parameterized in terms of  $\theta$ , the parameter of the simulator that defines the position of the nails (i.e. they take  $\theta$  as an input). We use a simple network architecture with a single hidden layer, 10 hidden units, and tanh activations. Figure 3 shows the mean squared error between  $\log \hat{r}(x|\theta_0, \theta_1)$  and the true  $\log r(x|\theta_0, \theta_1)$  (estimated from histograms of  $2 \cdot 10^4$  simulations from  $\theta_0 = -0.8$  and  $\theta_1 = -0.6$ ), summing over  $x \in [5, 15]$ , versus the training sample size (which refers to the total number of  $x$  samples, distributed over 10 values of  $\theta \in [-1, -0.4]$ ). We find that both SCANDAL and RASCAL are dramatically more sample efficient than pure neural density estimation and the likelihood ratio trick, which do not leverage the joint score. ROLR improves upon pure neural density estimation and achieves the same asymptotic error as SCANDAL, though more slowly.

## 5.2 Lotka-Volterra model

As a second example, we consider the Lotka-Volterra system [38, 39], a common example in the likelihood-free inference literature. This stochastic Markov jump process models the dynamics of a species of predators interacting with a species of prey. Four parameters  $\theta$  set the rate of four possible events: predators and prey being born, predators dying, and predators eating prey. While the evolution of this system can easily be simulated, the likelihood function is intractable.

We simulate the Lotka-Volterra model with Gillespie’s algorithm [40]. From the time evolution of the predator and prey populations we calculate summary statistics

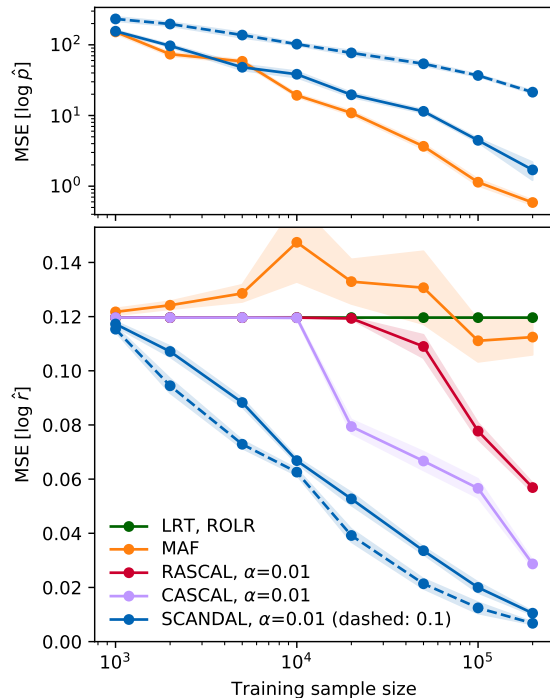


Figure 4: Lotka-Volterra example. MSE on  $\log p$  (top) and  $\log r$  (bottom) vs. training sample size. We show the median and the standard deviation of 10 runs.

istics  $x \in \mathbb{R}^9$ . Our model definitions, summary statistics, and initial conditions exactly follow Appendix F of Ref. [12]. In addition to the observations, we extract the joint score as well as the joint likelihood ratio with respect to a reference hypothesis  $\log \theta_1 = (-4.61, -0.69, 0.00, -4.61)^T$  from the simulator. On this augmented data we train different likelihood and likelihood ratio estimators. As baselines we use CARL [9, 32] and a conditional masked autoregressive flow (MAF) [22, 41]. We compare them to the new techniques introduced in section 4.2, including a SCANDAL likelihood estimator based on a MAF. For MAF and SCANDAL we stack four masked autoregressive distribution estimators (MADEs) [7] on a mixture of MADEs with 10 components. This “MAF MoG” architecture [22] performs better than a flow based on a single Gaussian base density. For all other methods, we use three hidden layers. In all cases, the hidden layers have 100 units and tanh activations. Code for simulation and inference is available at Ref. [42].

For inference on a wide prior in the parameter space, the different probability densities often do not overlap. As discussed above, the augmented data is then of limited use. Instead, we focus on the regime where we try to discriminate between close parameter points with similar predictions for the observables. We generate training data and evaluate the models in the range

$\log(\theta_1)_i - 0.01 \leq \theta_i \leq \log(\theta_1)_i + 0.01$  with a uniform prior in log space. In Fig. 4 we evaluate the different methods by calculating the mean squared error of estimators trained on small training samples. Since the true likelihood is intractable, we calculate the error with respect to the median predictions of 10 estimators<sup>1</sup> trained on the full data set of 200 000 samples.

Our results indicate a trade-off between the performance in likelihood (density) estimation and likelihood ratio estimation. For density estimation, the MAF performs well. The variance of the score term in the SCANDAL loss degrades the performance, especially for larger values of the hyperparameter  $\alpha$  (see the dashed line in Fig. 4). However, for statistical inference the more relevant quantity is the likelihood ratio. Here the new techniques that use the joint score, in particular SCANDAL, are significantly more sample efficient.

### 5.3 Particle physics

Finally we consider a real-world problem from particle physics. A simulator describes the production of a Higgs boson at the Large Hadron Collider experiments, followed by the decay into four electrons or muons, subsequent radiation patterns, the interaction with the detector elements, and the reconstruction procedure. Each recorded collision produces a single high-dimensional observable  $x \in \mathbb{R}^{42}$ , and the dataset consists of multiple iid observations of  $x$ . The goal is to infer confidence limits on two parameters  $\theta \in [-1, 1]^2$  that characterize the effect of high-energy physics models on these interactions. We consider a synthetic observed dataset with 36 iid simulated observations of  $x$  drawn from  $\theta = (0, 0)$ .

The new inference techniques can accommodate state-of-the-art simulators, but in that setting we cannot compare them to the true likelihood function. We therefore present a simplified setup and approximate the detector response such that the true likelihood function is tractable, providing us with a ground truth to compare the inference techniques to. As simulator we use a combination of MADGRAPH 5 [43] and MAD-MAX [44–46]. The setup and the results of this experiment are described at length in Ref. [34]. We are able to extract the joint score and joint ratio from the simulation, and we test the sample efficiency and the quality of the inference for all of the new techniques

<sup>1</sup>We pick the algorithms we use for these “ground truth” predictions based on the variance between independent runs and the consistency of improvements with increasing training sample size. For likelihood estimation, we use the MAF as baseline, with qualitatively similar results when using SCANDAL. For likelihood ratio estimation, we use the SCANDAL estimator as baseline, and find qualitatively similar results for CASCAL.

except for SCANDAL.

In the left panel of Fig. 5 we show the expected mean squared error of the approximate  $\log \hat{r}(x|\theta_0, \theta_1)$  as a function of the training sample size. We take the expectation over random values of  $\theta_0$ , drawn from a Gaussian prior with mean  $(0, 0)$  and covariance matrix  $\text{diag}(0.2^2, 0.2^2)$ . We compare the new techniques to the traditional inference method in particle physics: estimating densities through histograms, using two established kinematic variables as summary statistics (similar to ABC).

All new inference techniques outperform the traditional histogram method, provided that the training samples are sufficiently large. Using augmented data substantially decreases the amount of training data required for a good performance: the RASCAL method, which uses both the joint ratio and joint score information from the simulator, reduces the amount of training data by two orders of magnitude compared to the CARL technique, which uses only the samples  $x \sim p(x|\theta)$ . The particularly simple local techniques SALLY and SALLINO need even less data for a good performance. However, their performance eventually plateaus and does not asymptote to zero error. This is because the local model approximation breaks down further away from the reference point  $\theta_{\text{ref}} = (0, 0)^T$ , and the score is no longer the sufficient statistics. The resulting expected confidence intervals, in the right panel of Fig. 5, show that the CASCAL and RASCAL techniques have the highest precision, leading to exclusion limits virtually indistinguishable from those based on the true likelihood ratio.

## 6 Conclusions

In this work we have presented a range of new inference techniques for the setting in which the likelihood is only implicitly defined through a stochastic generative simulator. The new methods estimates likelihoods or ratios of likelihoods with data available from the simulator.

Most established inference methods, such as ABC and techniques based on neural density estimation, only use samples of observables from the simulator. We pointed out that in many cases the simulator also provides access to the joint likelihood ratio or the joint score, quantities conditional on the latent variables that characterize the data generation process. This scenario is common in the physical sciences, for instance in particle physics and cosmology.

While these additional quantities often require work to be extracted, they also prove to be very valuable as they can dramatically improve sample efficiency and



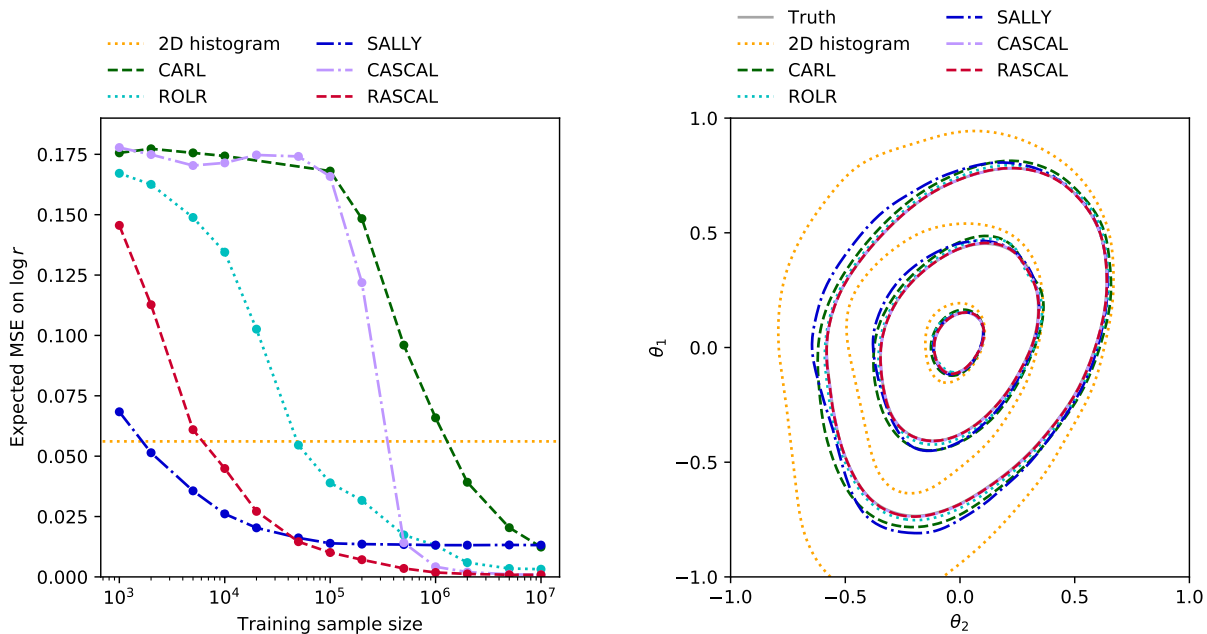


Figure 5: Particle physics example. Left: MSE on  $\log r$  vs. training sample size. Right: expected 68% / 95% / 99.7% confidence intervals for  $\theta$ , including ground truth (grey).

quality of inference. Indeed, we have shown that this additional information lets us define loss functionals that are minimized by the likelihood ratio, which can in turn be used to efficiently guide the training of neural networks to precisely estimate likelihood ratios. This is the idea behind the new ROLR, CASCAL, RASCAL, and SCANDAL inference techniques, which are differentiated by which pieces of information they incorporate.

A second class of new techniques is motivated by a local approximation of the likelihood function around a reference point, where the score vector are the sufficient statistics. In the case where the simulator provides the joint score, we can use it to train a precise estimator of the score and use it as optimal summary statistics. We introduce the SALLY and SALLINO techniques, which estimate likelihood ratios through density estimation in the estimated score space. This approach lets us compress any observation into a scalar function without losing information on the likelihood ratio, at least in the local approximation.

We have demonstrated in three experiments that the new inference techniques let us precisely estimate likelihood ratios. In turn, this enables parameter measurement with a higher precision and less training data than with established methods.

Finally, these results motivate the development of tools that provide a nonstandard interpretation of the simulator code and automatically generate the joint score and joint ratio. These tools could borrow from recent developments in probabilistic programming and auto-

matic differentiation [29, 30, 47–50]. Such tools would reduce the effort needed to mine the gold so valuable to simulator-based inference.

## Acknowledgments

We would like to thank Cyril Becot and Lukas Heinrich, who contributed to this project at an early stage. We are grateful to Felix Kling, Tilman Plehn, and Peter Schichtel for providing the MADMAX code and helping us use it, and to George Papamakarios for discussing the Masked Autoregressive Flow code with us. KC wants to thank CP3 at UC Louvain for their hospitality. Finally, we would like to thank Atılım Güneş Baydin, Lydia Brenner, Joan Bruna, Kyunghyun Cho, Michael Gill, Siavash Golkar, Ian Goodfellow, Daniela Huppenkothen, Michael Kagan, Hugo Larochelle, Yann LeCun, Fabio Maltoni, Jean-Michel Marin, Iain Murray, George Papamakarios, Duccio Pappadopulo, Dennis Prangle, Rajesh Ranganath, Dustin Tran, Rost Verkerke, Wouter Verkerke, Max Welling, and Richard Wilkinson for interesting discussions.

JB, KC, and GL are grateful for the support of the Moore-Sloan data science environment at NYU. KC and GL were supported through the NSF grants ACI-1450310 and PHY-1505463. JP was partially supported by the Scientific and Technological Center of Valparaíso (CCTVal) under Fondecyt grant BASAL FB0821. This work was supported in part through the NYU IT High Performance Computing resources, services, and staff expertise.

## Bibliography

- [1] D. B. Rubin: ‘Bayesianly justifiable and relevant frequency calculations for the applied statistician’. *Ann. Statist.* 12 (4), p. 1151, 1984. URL <https://doi.org/10.1214/aos/1176346785>.
- [2] M. A. Beaumont, W. Zhang, and D. J. Balding: ‘Approximate bayesian computation in population genetics’. *Genetics* 162 (4), p. 2025, 2002.
- [3] J. Alsing, B. Wandelt, and S. Feeney: ‘Massive optimal data compression and density estimation for scalable, likelihood-free inference in cosmology’, 2018. arXiv:1801.01497.
- [4] T. Charnock, G. Lavaux, and B. D. Wandelt: ‘Automatic physical inference with information maximizing neural networks’. *Phys. Rev. D* 97 (8), p. 083004, 2018. arXiv:1802.03537.
- [5] Y. Fan, D. J. Nott, and S. A. Sisson: ‘Approximate Bayesian Computation via Regression Density Estimation’. ArXiv e-prints , 2012. arXiv:1212.1479.
- [6] L. Dinh, D. Krueger, and Y. Bengio: ‘NICE: Non-linear Independent Components Estimation’. ArXiv e-prints , 2014. arXiv:1410.8516.
- [7] M. Germain, K. Gregor, I. Murray, and H. Larochelle: ‘MADE: Masked Autoencoder for Distribution Estimation’. ArXiv e-prints , 2015. arXiv:1502.03509.
- [8] D. Jimenez Rezende and S. Mohamed: ‘Variational Inference with Normalizing Flows’. ArXiv e-prints , 2015. arXiv:1505.05770.
- [9] K. Cranmer, J. Pavez, and G. Louppe: ‘Approximating Likelihood Ratios with Calibrated Discriminative Classifiers’, 2015. arXiv:1506.02169.
- [10] K. Cranmer and G. Louppe: ‘Unifying generative models and exact likelihood-free inference with conditional bijections’. *J. Brief Ideas* , 2016.
- [11] L. Dinh, J. Sohl-Dickstein, and S. Bengio: ‘Density estimation using Real NVP’. ArXiv e-prints , 2016. arXiv:1605.08803.
- [12] G. Papamakarios and I. Murray: ‘Fast  $\varepsilon$ -free inference of simulation models with bayesian conditional density estimation’. In ‘Advances in Neural Information Processing Systems’, p. 1028–1036, 2016.
- [13] B. Paige and F. Wood: ‘Inference Networks for Sequential Monte Carlo in Graphical Models’. ArXiv e-prints , 2016. arXiv:1602.06701.
- [14] R. Dutta, J. Corander, S. Kaski, and M. U. Gutmann: ‘Likelihood-free inference by ratio estimation’. ArXiv e-prints , 2016. arXiv:1611.10242.
- [15] B. Uria, M.-A. Côté, K. Gregor, I. Murray, and H. Larochelle: ‘Neural Autoregressive Distribution Estimation’. ArXiv e-prints , 2016. arXiv:1605.02226.
- [16] A. van den Oord, S. Dieleman, H. Zen, et al.: ‘WaveNet: A Generative Model for Raw Audio’. ArXiv e-prints , 2016. arXiv:1609.03499.
- [17] A. van den Oord, N. Kalchbrenner, O. Vinyals, L. Espeholt, A. Graves, and K. Kavukcuoglu: ‘Conditional Image Generation with PixelCNN Decoders’. ArXiv e-prints , 2016. arXiv:1606.05328.
- [18] A. van den Oord, N. Kalchbrenner, and K. Kavukcuoglu: ‘Pixel Recurrent Neural Networks’. ArXiv e-prints , 2016. arXiv:1601.06759.
- [19] M. U. Gutmann, R. Dutta, S. Kaski, and J. Corander: ‘Likelihood-free inference via classification’. *Statistics and Computing* p. 1–15, 2017.
- [20] D. Tran, R. Ranganath, and D. M. Blei: ‘Hierarchical Implicit Models and Likelihood-Free Variational Inference’. ArXiv e-prints , 2017. arXiv:1702.08896.
- [21] G. Louppe and K. Cranmer: ‘Adversarial Variational Optimization of Non-Differentiable Simulators’. ArXiv e-prints , 2017. arXiv:1707.07113.
- [22] G. Papamakarios, T. Pavlakou, and I. Murray: ‘Masked Autoregressive Flow for Density Estimation’. ArXiv e-prints , 2017. arXiv:1705.07057.
- [23] C.-W. Huang, D. Krueger, A. Lacoste, and A. Courville: ‘Neural Autoregressive Flows’. ArXiv e-prints , 2018. arXiv:1804.00779.
- [24] G. Papamakarios, D. C. Sterratt, and I. Murray: ‘Sequential Neural Likelihood: Fast Likelihood-free Inference with Autoregressive Flows’. ArXiv e-prints , 2018. arXiv:1805.07226.
- [25] W. Grathwohl, R. T. Q. Chen, J. Bettencourt, I. Sutskever, and D. Duvenaud: ‘FFJORD: Free-form Continuous Dynamics for Scalable Reversible Generative Models’. ArXiv e-prints , 2018. arXiv:1810.01367.
- [26] S. Mohamed and B. Lakshminarayanan: ‘Learning in Implicit Generative Models’. ArXiv e-prints , 2016. arXiv:1610.03483.
- [27] E. Meeds, R. Leenders, and M. Welling: ‘Hamiltonian abc’. arXiv preprint arXiv:1503.01916 , 2015.
- [28] M. M. Graham, A. J. Storkey, et al.: ‘Asymptotically exact inference in differentiable generative models’. *Electronic Journal of Statistics* 11 (2), p. 5105, 2017.
- [29] F. Wood, J. W. van de Meent, and V. Mansinghka: ‘A new approach to probabilistic programming inference’. In ‘Proceedings of the 17th International

- conference on Artificial Intelligence and Statistics’, p. 1024-1032, 2014.
- [30] T. A. Le, Baydin, A. G. Baydin, and F. Wood: ‘Inference compilation and universal probabilistic programming’. In ‘Proceedings of the 20th International Conference on Artificial Intelligence and Statistics (AISTATS)’, volume 54 of Proceedings of Machine Learning Research, p. 1338–1348. PMLR, Fort Lauderdale, FL, USA, 2017.
- [31] I. J. Goodfellow, J. Pouget-Abadie, M. Mirza, et al.: ‘Generative Adversarial Networks’. ArXiv e-prints , 2014. arXiv:1406.2661.
- [32] G. Louppe, K. Cranmer, and J. Pavez: ‘carl: a likelihood-free inference toolbox’. J. Open Source Softw. , 2016.
- [33] J. Brehmer, K. Cranmer, G. Louppe, and J. Pavez: ‘Constraining Effective Field Theories with Machine Learning’. Phys. Rev. Lett. 121 (11), p. 111801, 2018. arXiv:1805.00013.
- [34] J. Brehmer, K. Cranmer, G. Louppe, and J. Pavez: ‘A Guide to Constraining Effective Field Theories with Machine Learning’. Phys. Rev. D98 (5), p. 052004, 2018. arXiv:1805.00020.
- [35] J. Brehmer, K. Cranmer, G. Louppe, and J. Pavez: ‘Code repository for the generalized Galton board example in the paper “Mining gold from implicit models to improve likelihood-free inference”’. <http://github.com/johannbrehmer/simulator-mining-example>, 2018.
- [36] R. J. Williams: ‘Simple statistical gradient-following algorithms for connectionist reinforcement learning’. In ‘Reinforcement Learning’, Springer, p. 5–32, 1992.
- [37] P. Baldi, K. Cranmer, T. Fausett, P. Sadowski, and D. Whiteson: ‘Parameterized neural networks for high-energy physics’. Eur. Phys. J. C76 (5), p. 235, 2016. arXiv:1601.07913.
- [38] A. J. Lotka: ‘Analytical note on certain rhythmic relations in organic systems’. Proceedings of the National Academy of Sciences 6 (7), p. 410, 1920.
- [39] A. J. Lotka: ‘Undamped oscillations derived from the law of mass action.’ Journal of the american chemical society 42 (8), p. 1595, 1920.
- [40] D. T. Gillespie: ‘A general method for numerically simulating the stochastic time evolution of coupled chemical reactions’. Journal of Computational Physics 22 (4), p. 403 , 1976.
- [41] G. Papamakarios, T. Pavlakou, and I. Murray: ‘Code repository for paper “Masked Autoregressive Flow for Density Estimation”’. <http://github.com/gpapamak/maf>, 2017.
- [42] J. Brehmer, K. Cranmer, G. Louppe, and J. Pavez: ‘Code repository for the Lotka-Volterra example in the paper “Mining gold from implicit models to improve likelihood-free inference”’. <http://github.com/johannbrehmer/goldmine>, 2018.
- [43] J. Alwall, R. Frederix, S. Frixione, et al.: ‘The automated computation of tree-level and next-to-leading order differential cross sections, and their matching to parton shower simulations’. JHEP 07, p. 079, 2014. arXiv:1405.0301.
- [44] K. Cranmer and T. Plehn: ‘Maximum significance at the LHC and Higgs decays to muons’. Eur. Phys. J. C51, p. 415, 2007. arXiv:hep-ph/0605268.
- [45] T. Plehn, P. Schichtel, and D. Wiegand: ‘Where boosted significances come from’. Phys. Rev. D89 (5), p. 054002, 2014. arXiv:1311.2591.
- [46] F. Kling, T. Plehn, and P. Schichtel: ‘Maximizing the significance in Higgs boson pair analyses’. Phys. Rev. D95 (3), p. 035026, 2017. arXiv:1607.07441.
- [47] B. Eli, J. P. Chen, M. Jankowiak, et al.: ‘Pyro: Deep probabilistic programming’. <https://github.com/uber/pyro>, 2017.
- [48] D. Tran, M. D. Hoffman, R. A. Saurous, E. Brevdo, K. Murphy, and D. M. Blei: ‘Deep probabilistic programming’. arXiv preprint arXiv:1701.03757 , 2017.
- [49] N. Siddharth, B. Paige, J.-W. van de Meent, et al.: ‘Learning disentangled representations with semi-supervised deep generative models’. In I. Guyon, U. V. Luxburg, S. Bengio, et al. (eds.), ‘Advances in Neural Information Processing Systems 30’, p. 5927–5937. Curran Associates, Inc., 2017.
- [50] A. Gelman, D. Lee, and J. Guo: ‘Stan: A Probabilistic Programming Language for Bayesian Inference and Optimization’. Journal of Educational and Behavioral Statistics 40 (5), p. 530, 2015.